AGU ADVANCING EARTH AND SPACE SCIENCES

JGR Space Physics

Key Points:

- A global network of portable muon detectors is under development for monitoring the dynamic changes of the space and terrestrial weather
- A comparison of the measured cosmic ray (CR) muon fluxes from two identical detectors at different geolocations in real-time is carried out
- A correlation study between the muon data and the neutron measurement at Oulu CR station in Finland is presented in this paper

Correspondence to:
A. Mubashir,
amubashir1@gsu.edu

Muon Flux Variations Measured by Low-Cost Portable Cosmic Ray Detectors and Their Correlation With Space Weather Activity

A. Mubashir[1] [ID], A. Ashok[2], A. G. Bourgeois[2], Y. T. Chien[1], M. Connors[1], E. Potdevin[1], X. He[1] [ID], P. Martens[1], A. Mikler[2], A. G. U. Perera[1], V. Sadykov[1], M. Sarsour[1], D. Sharma[1] [ID], and C. Tiwari[2,3]

[1]Department of Physics and Astronomy, Georgia State University, Atlanta, GA, US, [2]Department of Computer Science, Georgia State University, Atlanta, GA, US, [3]Department of Geosciences, Georgia State University, Atlanta, GA, US

Abstract We present a comparison of the measured cosmic ray (CR) muon fluxes from two identical portable low-cost detectors at different geolocations and their sensitivity to space weather events in real time. The first detector is installed at Mount Wilson Observatory, CA, USA (geomagnetic cutoff rigidity Rc ∼ 4.88 GV), and the second detector is running on the downtown campus of Georgia State University in Atlanta, GA, USA (Rc ∼ 3.65 GV). The variation of the detected muon fluxes is compared to the changes in the interplanetary solar wind parameters at the L1 Lagrange point and geomagnetic indexes. In particular, we have investigated the muon flux behavior during three major interplanetary shock events and geomagnetic disturbances that occurred during July and August of 2022. To validate the interpretation of the measured muon signals, we compare the muon fluxes to the measurement from the Oulu neutron monitor (NM, Rc ∼ 0.8 GV). The results of this analysis show that the muon detector installed at Mount Wilson Observatory demonstrates a stronger correlation with a high-latitude NM. Both detectors typically observe a muon flux decrease during the arrival of interplanetary shocks and geomagnetic storms. Interestingly, the decrease could be observed several hours before the onset of the first considered interplanetary shocks at L1 at 2022-07-23 02:28:00 UT driven by the high-speed Coronal Mass Ejection and related geomagnetic storm at 2022-07-23 03:59:00 UT. This effort represents an initial step toward establishing a global network of portable low-cost CR muon detectors for monitoring the sensitivity of muon flux changes to space and terrestrial weather parameters.

Plain Language Summary A pair of identical, low-cost, and portable cosmic ray (CR) muon detectors is set up over 3,500 km apart for an exploratory study of monitoring space and terrestrial weather in real time at a global scale. One detector is installed on Mount Wilson, California and the other is in downtown Atlanta, Georgia. To validate the interpretation of the measured muon signals, the muon fluxes are compared to the well-known neutron flux measurement from the Oulu neutron station in Finland. The results of this analysis show that the CR flux from both muon detectors typically decreases during geomagnetic storm events and that the muon detector installed on Mount Wilson is significantly correlated with the Oulu neutron monitor. Although this is yet an initial effort of building a global network of CR muon detectors for monitoring the space and earth weather in real time, the study provides evidence that muon network detection efficiency can be sufficient for a diagnostic of the major geoeffective space weather events.

1. Introduction

Understanding the interplay between solar activity, solar and extrasolar energetic particles, the interplanetary solar wind plasmas and its magnetic field, and the Earth's magnetosphere is crucial for monitoring and predicting space weather. This dynamic interaction involves the solar wind carrying frozen-in magnetic fields and cosmic ray (CR) particles within the interplanetary space. Solar wind modulates the incoming CR flux through diffusion, drift processes, and adiabatic cooling (Parker, 1958). Changes in the solar wind and the propagation of the Coronal Mass Ejections (CMEs) cause the magnetosphere of the Earth to react as well (Storini, 1990), which affect the amount of CR particles incident at the Earth's atmosphere and detected at the ground level. For example, at least 86% of the CR measurement decreases observed by ground-based neutron monitors during 1964–1994 are attributed to CME-driven geomagnetic storms (Cane & Richardson, 2003; Cane et al., 1996; Kudela & Brenkus, 2004). Therefore the changes in the ground-level CR fluxes carry essential information about geomagnetic disturbances, solar eruptive events, and the solar wind, and may be used for the development of diagnostics and forecasting

(1) Primary cosmic ray particles mostly have galactic origin. Solar energetic particles (mainly protons) can contribute as well.

(2) Amount of cosmic ray particles reaching the top of the earth atmosphere is affected by the solar activity and the state of the magnetic field.

Geomagnetic field lines

Zoom in cosmic ray shower

(3) Secondary cosmic ray particle production in atmosphere at ~15 km

These ionizing particles are regarded as health hazards for flight crew.

Cloud formation

lightning

(4) Most particles reaching to the surface of earth are muon particles together with a few percent of neutrons. Measuring muon flux variation around the world allows us to monito the state of space weather and atmospheric properties in real-time, and to explore the associated applications of using cosmic rays (cloud formation, lightning, etc.)
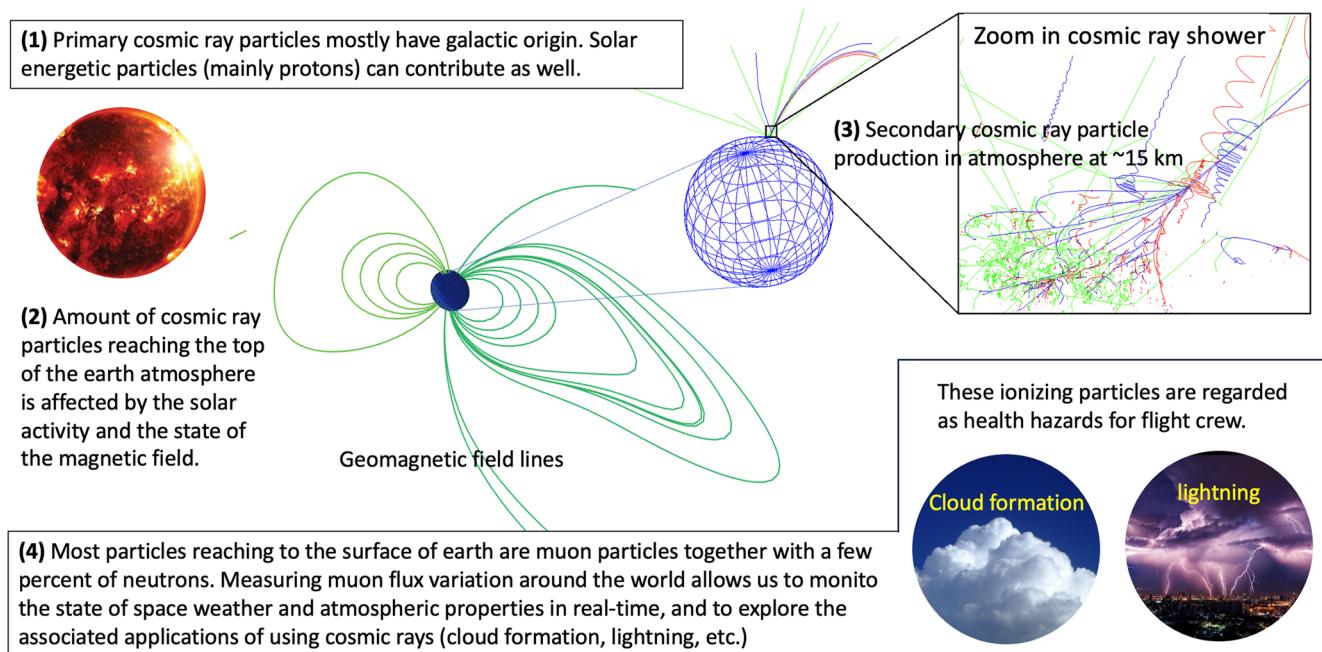
Figure 1. From the origin of cosmic rays to their detection on Earth. The dynamic state of the space weather and the atmospheric properties are encoded in the fluctuations of the cosmic ray flux.

tools. These modulations have significant implications for space weather forecasting (Gleeson & Axford, 1968; Kojima et al., 2015) affecting our society by both rare and dangerous solar transient events, as well as on a more ordinary, sometimes everyday, basis (Guhathakurta, 2021).

High-energy particles can be produced during the solar transient activity events (so-called *solar energetic particles*, i.e., SEPs, Reames, 2021) and can be coming from outside the solar system (so-called primary *CR particles*). Figure 1 highlights the four major processes of CR propagation and interactions with the interplanetary and terrestrial environments. The primary CR particles mostly have galactic or solar origins. The GeV-TeV particles enter into the heliosphere or are injected/accelerated near the Sun. Some of them pass the Earth's magnetosphere and continue traversing the Earth's atmosphere toward the surface of the Earth interacting with atmospheric molecules and developing secondary CR particles. These secondary particles, in turn, interact with the surrounding atmospheric particles, creating an even more extended shower of particles. As the CR showers develop, the number of secondary particles increases until it reaches a maximum at a specific altitude known as the "Regener-Pfotzer maximum." The altitude of the Regener-Pfotzer maximum is typically around 20–25 km above the Earth's surface. At this altitude, the decrease in atmospheric density balances the decrease in the flux of cosmic rays, resulting in a peak in the CR intensity. The exact altitude of the Regener-Pfotzer maximum can vary depending on various factors, such as solar activity, the energy of the cosmic rays, and the dynamic properties of the atmosphere. The interactions of the primary and secondary CR particles with the atmosphere can lead to ionization, which influences the electrical properties of clouds, may indirectly affect lightning formation, and cause public health concerns (Svensmark et al., 2021).

The most abundant CR shower particles reaching sea level are muons (about 80%, Zyla et al., 2020) together with a few percent of neutrons and electrons (ignoring neutrino particles which are irrelevant for this study). The solar activity, the state of the interplanetary space, and the Earth's magnetosphere and atmosphere are collectively responsible for the intensity of secondary CR particles being detected by ground-based CR detectors. Studies of correlations between the CR flux and solar activity parameters (Dvornikov et al., 1988; Firoz et al., 2010; Maghrabi et al., 2021; Munakata et al., 2000) reveal that disturbances in the solar wind and interplanetary CME shocks, as well as the enhancements of the solar energetic particle fluxes, may result in geomagnetic activity and CR modulation. Because the number of solar energetic particle events that resulted in the Ground Level Enhancement is small (16 events during the solar cycle 23, (Gopalswamy et al., 2012), and only 2 events during the solar cycle 24), the two main phenomena responsible for the modulation of the flux rate of cosmic rays incident on

the Earth's upper atmosphere and detected on the ground are then the disturbances in the solar wind and the state of Earth's magnetic field (Firoz et al., 2010; Kudela et al., 1993). This modulation of cosmic rays can be analyzed by the peaks and valleys in their time series detected by ground-based particle detectors (Shrivastava & Jaiswal, 2003). Thus, The study of the CR muon flux is crucial in increasing our knowledge of solar activity and solar-terrestrial interactions, potentially contributing to the safety of spacecraft and astronauts, advancing scientific research, and improving models of space weather, all of which leads to better understanding of space weather impacts on technology and infrastructure. Variations in CR muon fluxes can serve as a tool for space weather prediction and provide early warning signs of high solar activities and geomagnetic storms.

Knowledge of short-term CR modulation on a large scale is of great importance because of its correlation with various solar, interplanetary, and geophysical parameters (Sabbah, 2000). The international collaborations of the Global Muon Detector Network (De Mendonça et al., 2016; Munakata et al., 2018, GMDN) and the NM Network and related Database are aimed at studying CR measurement in high precision. These networks provide access to ground-based muon detectors (including Japan, Australia, Brazil, and Kuwait) and NM measurements (including USA, Canada, Germany, France, etc, and the locations both north and south at the very low geomagnetic cutoff rigidities) from stations around the world. GMDN offers valuable insights into cosmic muon phenomena, allowing scientists to study various aspects of particle physics and astrophysics. But establishing, maintaining, and operating a global network of such large ground muon detectors can be costly. Also, challenges in relation to portability and fast deployment (i.e., installation and quick validation tests) limit the number of locations where the detectors can be installed. The challenge in space and Earth weather monitoring on a global scale using cosmic rays started to be addressed in this paper is to develop efficient, low-cost, and portable detectors that can provide monitoring capabilities for CR flux variations and changes in solar activity and atmospheric properties.

Such a state-of-the-art portable muon particle detector has been developed by the Nuclear Physics Group at Georgia State University (GSU, He et al., 2021). An interdisciplinary team at GSU has successfully deployed its first remotely installed CR muon detector (to be referred to as Muon002) on Mount Wilson, CA on 7 June 2022. The site is the home of the Center for High Angular Resolution Astronomy (CHARA) Array, a flagship project of GSU's Center for High Angular Resolution Astronomy (CHARA). Such portable, low-cost muon detectors offer advantages in terms of accessibility, affordability, mobility, expansion, and rapid prototyping and innovation, making them an attractive option for researchers and enthusiasts interested in muon detection studies. This detector network effort is complementary to the existing GMDN facility units (De Mendonça et al., 2016; Munakata et al., 2018) and, while having a significantly smaller effective area, is based on another principle of the CR hit detection (silicon photomultipliers, SIPMs, compared to photomultiplier tubes, PMTs) and yet sensitive to the space and terrestrial weather effects as described in this paper. This marks the beginning of a long-term effort by the team to build a global network of such affordable and low-maintenance CR muon detectors for monitoring space and terrestrial weather. This network could become a significant asset for statistical and case studies of muon flux variations preceding and happening during geomagnetic storms. Moreover, some studies reveal that ground-based muon detectors can detect Earth-directed CMEs and interplanetary shock waves earlier than neutron monitors (Jansen et al., 2001; Munakata et al., 2000) based on the CR anisotropies caused by the interplanetary shock. The measurements by the identical muon detector installed at the GSU campus in downtown Atlanta (to be referred to as Muon000) provide a possibility to analyze the simultaneous response of both detectors to global magnetospheric disturbances and solar events.

The objective of this study is to perform an exploratory investigation of the response of in-house developed low-cost portable muon detectors to terrestrial weather variations and space weather events and investigate the short-term correlation of the CR muon and neutron flux variation with solar and geomagnetic activity. In particular, we report the first results of analyzing the time series of CR muon fluxes recorded by Muon000 (Atlanta, GA, USA) and Muon002 (Mount Wilson, CA, USA). The paper is divided into four sections. Section 2 presents the detector setup, data sources, and the associated data analysis details. The discussion of results is presented in Section 3 while Section 4 concludes the paper.

2. Detector Setup and Data Set Sources

2.1. Cosmic Ray Muon Detector Design and Configuration

The development of the present baseline CR muon detector (shown in Figure 2) took about 10 years with multiple iterations of prototyping and testing. The important design goals include (a) minimizing the total cost; (b)
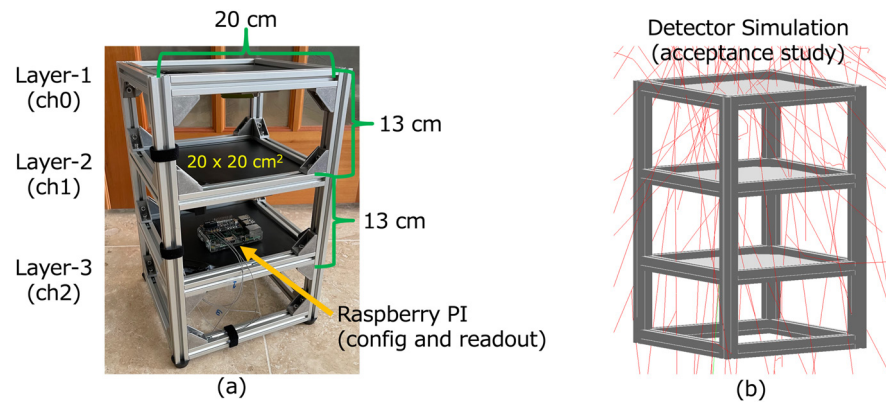
Figure 2. Desktop cosmic ray (CR) muon detector design: (a) CR muon detector dimension and configuration; the baseline muon detector setup with the adjacent scintillator layers 13 cm apart (b) Detector acceptance study using GEANT4 simulation toolkit.

portability for remote deployment; and (c) the hourly data sample should have sufficient statistical precision for responding to the space weather events and the changes of the terrestrial weather patterns. The key detector components consist of three layers of $20 \times 20 \times 1$ cm plastic scintillator tiles with embedded wavelength shifting fibers for efficiently collecting scintillation light using a silicon photomultiplier. The latter was inspired by the design of the sPHENIX Experiment at Brookhaven National Lab that three members of the authors were heavily involved from 2016 to 2022. The readout is done using a custom-made PCB which is mounted to a Raspberry PI (a low-cost, credit-card-size, and full-fledged computer). In the baseline design of the cosmic muon detector (see Figure 2), the three scintillating tiles are supported by an extruded aluminum frame for stability and flexible reconfiguration. The separation distance between layers 1 and 2 is equal to the distance between layers 2 and 3, which allows us to make a quick check of the detector performance since one is expecting equal average coincidence counts between layers 1 & 2 and layers 2 & 3. Once the detector is powered up, the control software running on the Raspberry PI automatically configures detector settings and starts recording the coincidence counts in layers 1 & 2, 1 & 3 and 2 & 3, respectively, at any configurable time interval. In a normal operation setting, the counts are recorded in every minute continuously unless there is a power failure or a need for maintenance checks. One of the longest-running periods of one detector lasted about 18 months. The recorded data are automatically transmitted to a data server located at GSU for data quality monitoring and offline data analysis. An example of the analyses includes the time-series comparison against the local barometric pressure and the ground temperature as shown in Figure 4. A remarkable anti-correlation between the percent-change of the hourly muon counts and the barometric pressure is seen, which is a well-known phenomenon in the community of CR measurement and demonstrates the statistical precision of our detectors. The CR flux near the surface of the earth varies with geoposition and the changes in the local weather conditions. As expected, our detectors installed in Sri Lanka and Columbia, which are close to the equator region, record less flux (about 100 counts per minute) in comparison with the measurements at higher latitudes like in Atlanta and in California (over 200 per minute). One should expect an even higher flux rate closer to the pole region. At a given location, the muon flux can be approximated by a Poisson distribution. For a minute-count rate at 100, the statistical precision of the hourly count is about 1.3% ($= 1/\sqrt{60 \times 100}$). The precision is getting better for the measurements at higher altitudes, which is sufficient for the exploratory study of the sensitivity of the low-cost and portable CR muon network to the space weather event at a global scale if one properly corrects the effect of regional terrestrial weather.

In this exploratory study, we focus on analyzing data recorded from two detectors. One of the detectors running on the GSU campus (to be referred to as Muon000) is installed on the 4th floor of a 5-floor building. Its GPS coordinate is 33° 44′ 56.38″ N in latitude and 84° 23′ 16.74″ W in longitude with cutoff rigidity $R_c \sim 3.65$ GV. The second detector was installed at the CHARA site on Mount Wilson on 7 June 2022 (to be referred to as Muon002). Its GPS position is 33° 30′ 13.10″ N in latitude and 150° 22′ 37.37″ W in longitude with an elevation of 1,742 m and cutoff rigidity $R_c \sim 4.88$ GV, as shown in Figure 3.

Cosmic ray flux is recorded every minute by both detectors and hourly data is then used in the present study. Hourly pressure and temperature data for the considered period are downloaded from automated weather
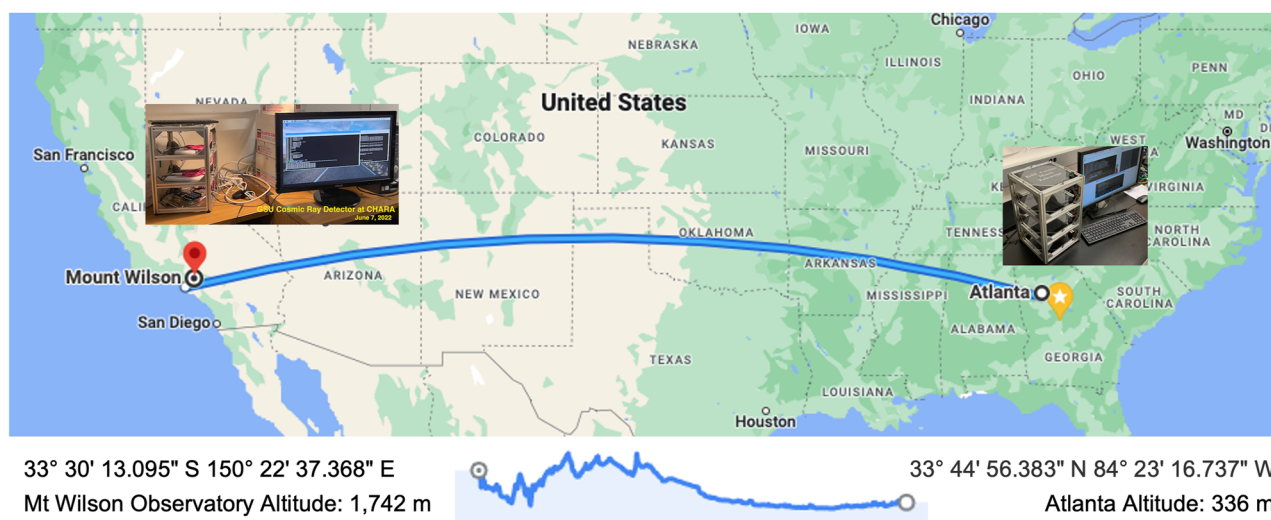
33° 30' 13.095" S 150° 22' 37.368" E
Mt Wilson Observatory Altitude: 1,742 m

33° 44' 56.383" N 84° 23' 16.737" W
Atlanta Altitude: 336 m

Figure 3. Cosmic ray muon detectors included in this study. The two detectors are ~3,500 km apart. The altitude of the detector on Mount Wilson is 1,742 m and a higher muon flux is recorded in this detector in comparison with the recorded muon flux in Atlanta.

observations provided by Iowa State University (Mesonet(IEM), 2023) used for the pressure and temperature correction of muon counts. In our research, we have recognized the significance of terrestrial weather effects on muon detection. To address this, we have incorporated the dependencies from ground-level temperature and pressure into the calibration process of our detector. For comparison of muon flux versus neutron flux, another data set used in this study is NM counts from Oulu (65.05°N, 25.47°E) which is one of the well-known and stable neutron detector stations actively measuring neutron flux on the ground level. Oulu data is publicly available online (University of Oulu, 2023).

2.2. Solar Activity and Wind Parameters

The solar wind and geomagnetic parameters used in this study are solar wind plasma speed, density, B_z component of Interplanetary Magnetic Field (IMF) determined in Geocentric Solar Magnetospheric coordinate system, and kinetic energy, as well as magnetospheric planetary K_p index and disturbance storm time Dst index (Cane & Richardson, 2003; Mishra & Mishra, 2018). Data has been obtained from the Low-Resolution OMNI data set of NASA's catalog (SPDF, 2023) Interplanetary shocks information for the considered period of study is taken from
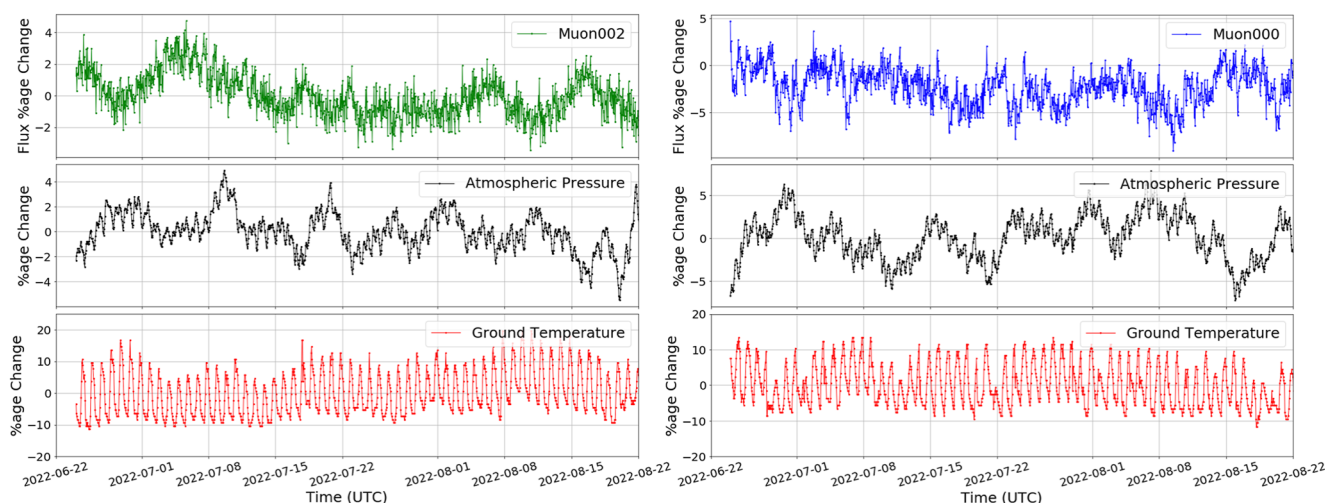

Figure 4. Plot of the percentage change in hourly counts for Muon000 and Muon002 over a period of time together with the percentage change of atmospheric pressure and ground level temperature.

the Database Of Notifications, Knowledge, Information (DONKI) developed at NASA Community Coordinated Modeling Center (DONKI at CCMC (NOAA, 2023)) and a news archive of Space Weather Prediction Center at National Oceanic and Atmospheric Administration (SWPC NOAA) (SWPC NOAA, 2023).

3. Data Analysis

To quantify the CR flux modulations, it is important to have knowledge of variations in solar and interplanetary parameters (Belov et al., 2005). The measured CR flux at the ground level depends on the intensity of CR flux above the Earth's atmosphere and the atmospheric profile at the detector location. The atmospheric thickness is directly associated with the local pressure measurements at the detector location (Kobelev et al., 2011). In order to explore the sensitivity to space weather-related processes and to represent the galactic CR intensities, applying pressure correction and temperature correction on data is a prerequisite (Dorman, 2004; Koldobskiy et al., 2022). In this work, we utilize the atmospheric pressure and ground-level temperature measurements, correlate them with the muon flux, and correct the latter for the atmospheric variation effects. Also, studying the geomagnetic variations along with muon flux measurements can help disentangle the effects of space weather from atmospheric influences. Geomagnetic indexes, such as Kp or Dst, reflect the global state of the Earth's magnetic field and can serve as indicators of geomagnetic disturbances caused by space weather events. Analyzing the correlation between geomagnetic variations and muon flux variations can help establish a link between space weather and observed modulations.

3.1. Atmospheric Effect on Muon Flux and Temperature and Pressure Correction

While our focus for this particular paper is on space weather effects, we are compensating for some atmospheric effects in our muon data by applying temperature and pressure corrections. Measured muon flux can be influenced by various local atmospheric factors such as changes in atmospheric density due to temperature and pressure. When atmospheric pressure is elevated, there is an increased amount of air mass that cosmic rays must traverse before reaching the Earth's surface. Hence, secondary CR particles are forming effectively at the higher heights, resulting in a decrease of measured CR fluxes at the ground because of the larger distances to travel and given the limited lifetime (∼2.2 μs). This results in an anti-correlation between CR rates and ground-level pressure. High temperatures also cause the atmosphere to expand, causing the same effect (anti-correlation) between the temperature and muon flux at the ground level. While both the temperature and pressure effects are intertwined, we are performing a two-step correction procedure in this work, when the first correction is applied for the quantity which experiences the highest correlation with the muon flux.

By accounting for these environmental factors, we can isolate and analyze the specific impact of space weather on the observed muon flux changes. The very first step of the data analysis is to look at the time series of the recorded CR counts and to identify the events of interest with the large decrease in the counts. Both Muon000 and Muon002 record muon counts in one-minute intervals. We sum the per-minute counts into hourly counts and then calculate the percentage changes of the hourly counts from the mean. The plot in Figure 4 shows the time series of hourly muon flux (i.e., the coincidence counts between layers) percent change. Also shown in the plot are the percent changes of the local atmospheric pressure and temperature at ground level, which clearly demonstrate the well-known and classic trend of the correlation between muon flux and pressure. Figure 5 shows the normalized percentage change of the hourly muon counts for both detectors together with the hourly ground level temperature and atmospheric pressure, at the location of the detectors, over a time period ranging from 24 June to 22 August 2022. The normalization is done by scaling the percentage change to the range of 0–1 using the Python built-in MinMaxScalar function. As it is shown in Figures 4 and 5, the muon fluxes from both detectors are in anti-correlation with the observed temperature and atmospheric pressure. The pressure variation is removed by using Equation 1 (Dorman, 2004; Kobelev et al., 2011; Koldobskiy et al., 2022)

$$N_{i,corr} = N_i e^{-\beta(P_i - P_o)}, \tag{1}$$

where N_i and $N_{i,corr}$ correspond to the recorded hourly and the pressure-corrected muon counts, respectively. P_i is the hourly atmospheric pressure and P_o represents the average pressure during the time period of this study. The barometric coefficient, β, is obtained by a least-squares linear regression model between $\ln\left(\frac{N_{i,corr}}{N_o}\right)$ and $(P_i - P_o)$. The β values obtained from the fit are −0.2%/mb and −0.06%/mb for Muon000 and Muon002, respectively. These
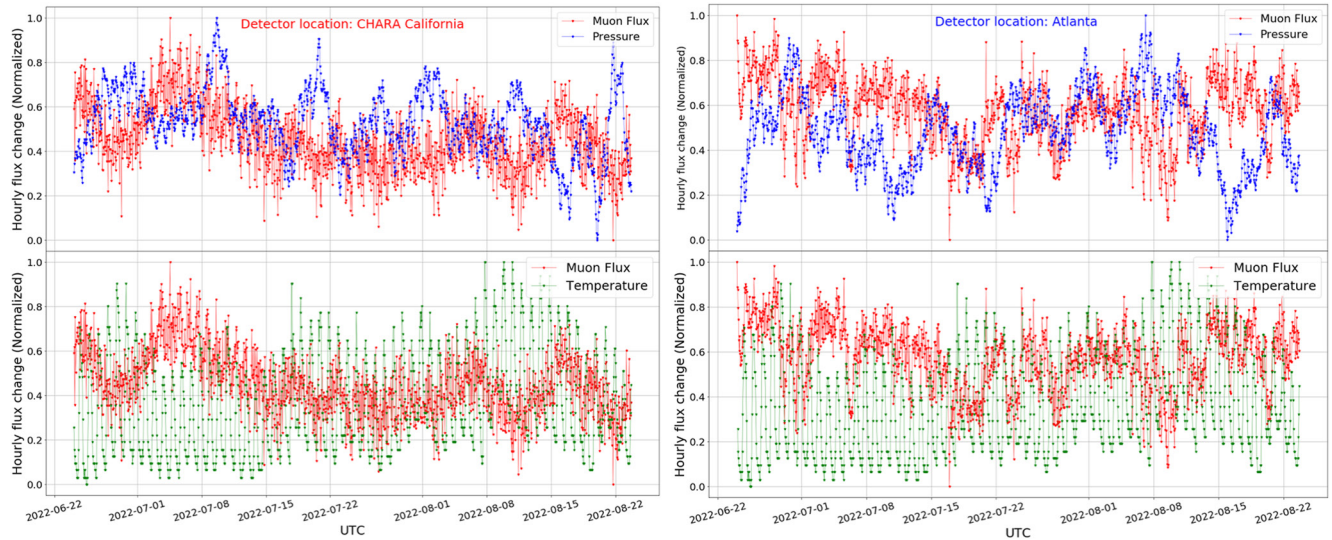
Figure 5. Normalized hourly muon flux percentage change (in red) time series of Muon002 and Muon000 overlaid with ground level temperature (in green) and atmospheric pressure (in blue). A clear trend of the well-known anti-correlation between the muon flux and the local ground level temperature and pressure is seen for both detectors.

values are close to the previously reported β-values (-0.114%/mb to -0.18%/mb) obtained from similar muons analyses reported in other works (Berkova et al., 2011; De Mendonça et al., 2013; Dmitrieva et al., 2013). We remove the effect of temperature variation on muon flux using Equation 2 (De Mendonça et al., 2016; Mendonça et al., 2019). The muon intensity variation expected due to the temperature effect ΔI_T as a linear function of temperature deviation close to the ground ΔT_{hGRD}

$$\Delta I_T = \alpha GRD * \Delta T_{hGRD}, \tag{2}$$

where αGRD is the ground temperature coefficient. It is well known that there is a seasonal variation of the muon flux, which is related to the expansion of the atmosphere to a higher altitude in the summer period. This study only covers a two-month period in the summer of 2022 and the seasonal temperature effect is therefore not considered. However, it is our intention to carry out seasonal effect analysis when more data (in a longer recording time period and with more detectors online) are available. This could be more important in the long-term data analysis, especially with the increasing global temperature associated with climate change.

3.2. Cross Comparison of Cosmic Ray Detector Data

As already stated in the introduction, the main objective of this study is to investigate the short-term correlation of the CR muon flux variations in a detector network with solar and geomagnetic activity.

Figure 6 shows the temperature and pressure-corrected percentage changes of the hourly muon counts from Muon000 and Muon002 in UTC time, plotted together with the pressure-corrected percentage change of the hourly neutron counts obtained from the Oulu neutron station for comparison. In the current reported time period of two months, the general trend of dips and peaks in the time series of neutron counts is in strong visual correlation with the flux percentage changes in Muon002 and is less evident in Muon000. To have a quantitative measure of how muon counts and neutron counts are related in a linear fashion, a Pearson correlation coefficient (r) was found between neutron and muon flux by using the formula:

$$r = \frac{\sum_{i=1}^{n}(x_i - \bar{x})(y_i - \bar{y})}{\sqrt{\sum_{i=1}^{n}(x_i - \bar{x})^2}\sqrt{\sum_{i=1}^{n}(y_i - \bar{y})^2}}, \tag{3}$$

where x_i, y_i correspond to data points in two data sets and $\bar{x}$, $\bar{y}$ are average values of two data sets, respectively.

The Pearson correlation coefficient found between Oulu versus Muon002, Oulu versus Muon000, and Muon002 versus Muon000 is 0.68, 0.20, and 0.25 respectively. When the Pearson correlation coefficient (r) approaches $+1$, the stronger the positive correlation. A Pearson correlation coefficient of 0.68 between Muon 002 and Oulu NM
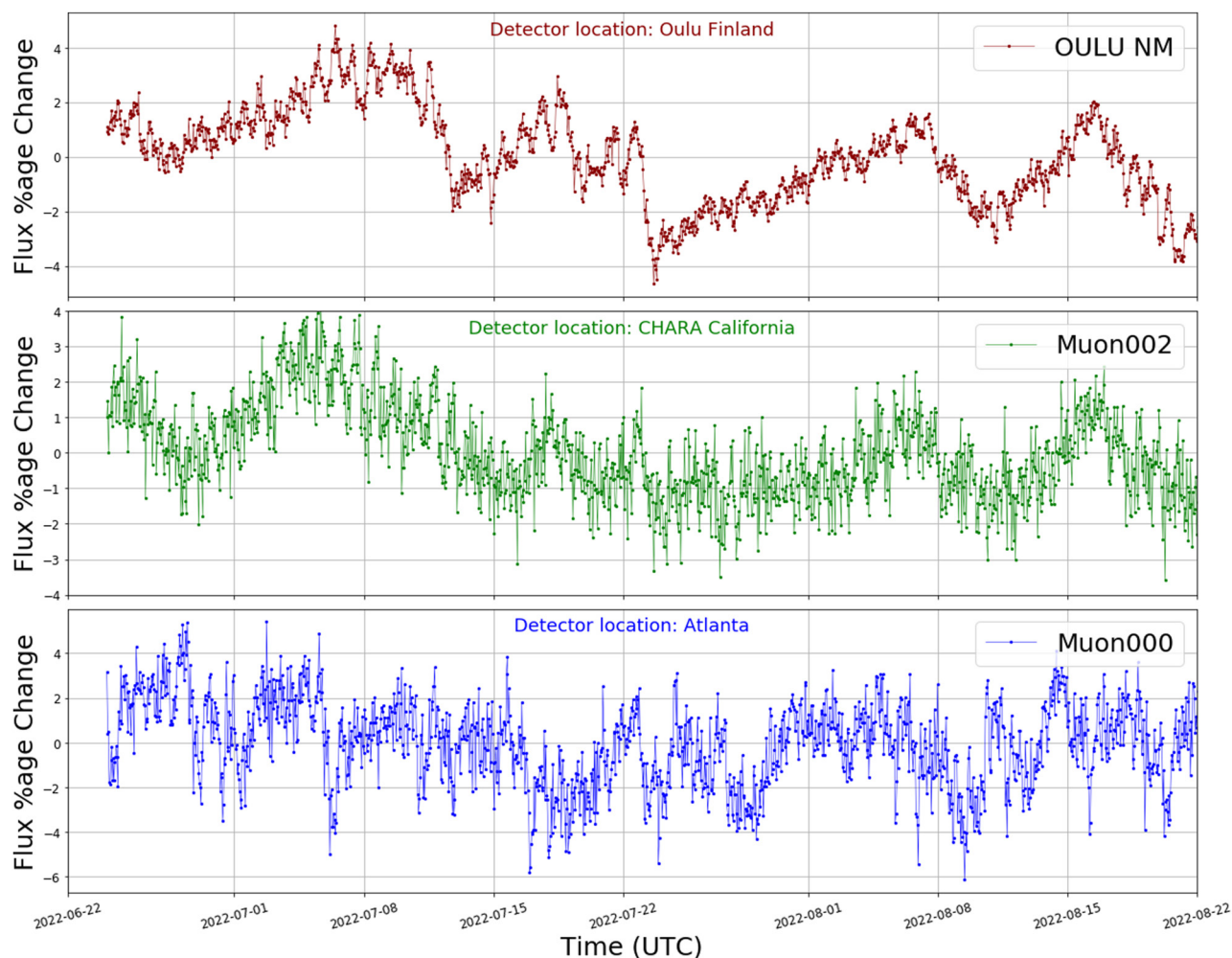
Figure 6. Comparative analysis of cosmic ray flux time series from the Oulu neutron station (top), Muon002 (middle), and Muon000 (bottom) after the atmospheric pressure and temperature correction.

indicates a strong and positive linear connection. To illustrate this correlation visually, a scatterplot Figure 7 for Oulu versus Muon 000 and Oulu versus Muon 002 demonstrates alignment with the interpretation of the Pearson correlation coefficient. The primary difference factor between Mount Wilson (Muon002) and Atlanta (Muon000) is that Muon002 is suited at a higher altitude of 1,740 m compared to 320 m of Atlanta.
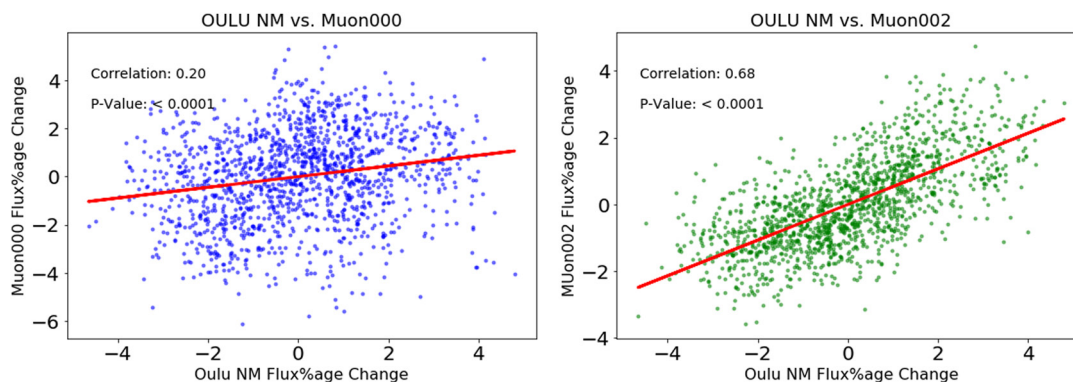

Figure 7. A correlation plot between muon data and neutron monitor data, As for Oulu versus Muon 002 (right plot), the points cluster around a straight line that slopes upward (positive correlation), this aligns with the interpretation of the Pearson correlation coefficient.

We believe that the stronger correlation between a high-altitude muon detector that is, Muon002, and a NM is presumably due to reduced column mass of the atmosphere and, as a result, fewer effects related to the terrestrial weather (the elevation of the detector at Mount Wilson is 1,741 m). At high altitudes, such detectors experience less impact of the thick, turbulent atmospheric layer that can greatly affect CR flux recorded by detectors installed at lower altitudes. In addition, the region around Mount Wilson experiences relatively stable atmospheric conditions, which enables both daytime (solar) and nighttime astronomical observations. Stable air minimizes the effects of temperature gradients and wind turbulence, which can cause fluctuations in the atmosphere and degrade viewing quality.

Another difference between Muon000 and Muon002 is the variability of their time series, which can also be attributed to the detector locations with different geomagnetic cut-off rigidities. For Oulu NM and Muon002, the percentage flux variability ranges around ±4%, while for Muon000% flux variability ranges around ±6%. It is evident from Figure 6 that for certain specific time periods, all detectors showed a continuous decrease in the flux percentage change. The decreasing trend in the form of negative dips can be related to space weather events which are explained in the next section.

3.3. Sensitivity of Muon Flux Variation to Space Weather Events

Solar activity causes variation in the CR flux that can have different magnitudes and different time scales based on the detector geolocations (Chaffer & Tedd, 2016; Maghrabi et al., 2021).

The evolution of the CR fluxes within the proximity of the interplanetary shocks and geomagnetic storm times is presented in more detail in Figure 8. Besides the muon and neutron fluxes, we highlight the time moments corresponding to the geomagnetic storms and interplanetary shocks according to the Space Weather DONKI, developed at the CCMC. We also tracked the news archive of SWPC NOAA for verifying the presence of these space weather events. Although DONKI contains only two geomagnetic storms in August 2022 (starting at 2022-08-07T21:00, and two subsequent storms at 2022-08-17T18:00 and 2022-08-18T00:00), we mark one more storm point at 2022-07-23T03:59 which corresponds to a high-Kp level as shown in Figure 8 and was reported (SWPC NOAA, 2023) by SWPC NOAA. Figure 6 covers a much broader time span from 2022-06-22 to 2022-08-22 for studying the correlation between detectors and their responses to fluctuations in atmospheric conditions such as temperature and pressure. In contrast Figure 8 focuses on a narrower time frame, from 2022-07-21 to 2022-08-21, to capture a period characterized by higher solar activity. The one-month 2022-06-22 to 2022-07-20 omission corresponds to a period of minimal solar activity and the absence of geomagnetic storms. This choice allows for a more targeted examination of the impact of increased solar activity on detectors and space parameters.

One of the prominent features seen in both detectors is the decrease of the CR intensity signals during the presence of interplanetary shocks and geomagnetic storms (Chaffer & Tedd, 2016). Specifically for the first event, observations seem to indicate a decrease in the muon fluxes that can be observed several hours ahead of the arrival at L1 of the first interplanetary shock on 2022-07-23T 02:28 (Day of year [DOY] 204) among the considered. For this event, DONKI indicates that the interplanetary shock and the related geomagnetic storm were caused by the high-speed CME (of the speed of 1,355 km/s as observed by coronagraph measurements). During the other two geomagnetic storms, GS on 2022-08-07 T21:00 (DOY 219) and GS on 2022-08-17 T18:00 (DOY 229), the decreases of muon flux can yet be seen in Muon 002 and are much less prominent in Muon000. We note here that the second event (minor geomagnetic storm) was due to high-speed stream effects with a peak solar wind speed of 668.0 km/s while for the third event, CME has a moderate speed of 817 km/s. The other observed dips in the data might be due to multiple causes, including space weather and terrestrial weather effects, even after corrections. One reason for a significant dip around 12 August 2022 could be a sudden increase in plasma temperature and elevated Kp index (Kp = 4). This occurred after a CME event on 6 August, accompanied by a sustained period of fast solar wind, though the exact cause remains uncertain. Also dip around 20 August 2022 might be linked with the multiple CMEs from the Sun, which started on August 14 and continued through August 16. Specific CME associations were noted, including IP = 2022-08-19 linked with a CME of a speed of 637 km/s and IP = 2022-08-20 linked with a high-speed CME of a speed of 1,313 km/s. Further statistical study with more events analyzed is required to confirm the presence of the muon flux decreases before the Interplanetary Coronal Mass Ejection (ICME) onset at L1. Yellow segmented bars in Figure 8 show the interval of ±12 hr with respect to the geomagnetic storm time, and two pink bars mark the same intervals for ICME events which were not related to any of the storm activities.

To quantify the level of sensitivity of the muon and neutron detectors to the interplanetary shocks (IP's) and geomagnetic storm events, we estimate the flux changing rate (i.e., slope) at each of the geomagnetic storms and
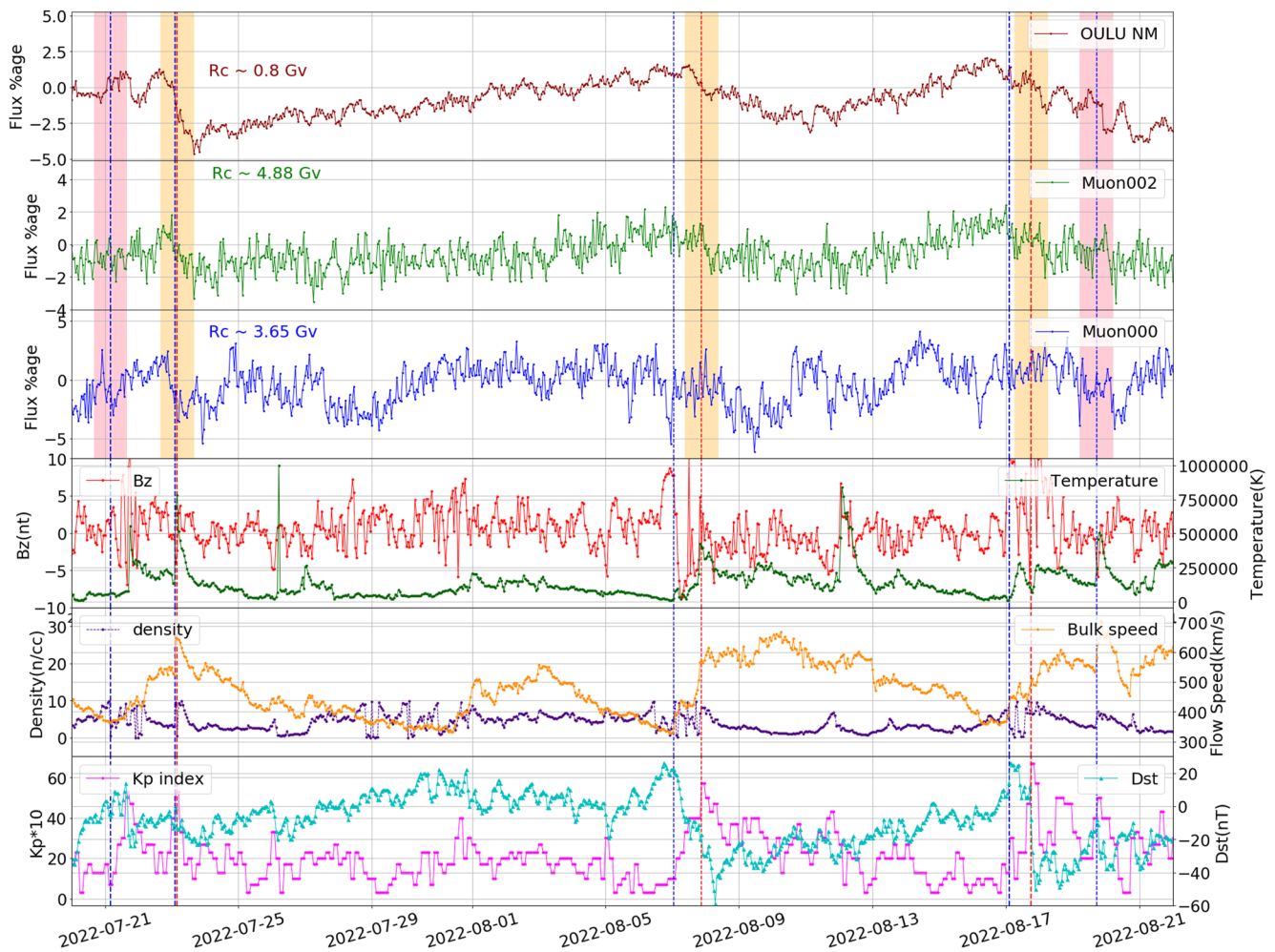
Figure 8. Time series of pressure and temperature corrected cosmic ray flux percentage changes and the space parameters from 2022-07-20T00:00 UT to 2022-08-22T00:00 UT. The vertical red dashed line within the shaded bars marks the times of the geomagnetic storm at 2022-07-23T03:59, 2022-08-7T21:00, and 2022-08-17T18:00 while vertical blue lines mark the Interplanetary Coronal Mass Ejection shocks (IP) at 2022-07-23T02:28, 2022-08-07T00:45, and 2022-08-17T02:14.

IPs with three time intervals in hours: ±12, ±6, and ±3. The flux change rates during these events for different time intervals are summarized in Tables 1 and 2. The presence of the preceding ICME shocks observed at L1 Lagrange Point by the Deep Space Climate Observatory (DSCOVR) and the solar drivers of the ICME shocks (coronal mass ejections, CMEs, or high-speed streams, HSS) is indicated in the footnotes of the table.

As seen in Tables 1 and 2, the computed slope values are negative for the first geomagnetic storm GS1 and during first interplanetary shock for all three detectors and all three time intervals considered. The observed slopes for the other two events, GS2/IP2 and GS3/IP3, are also mostly negative, but the calculated slopes (the rates of the flux change) are less steep. The qualitative change in slope results between the two tables remains unaffected whether the reference time is taken as the occurrence of a geomagnetic storm or an Interplanetary shock. After the occurrence of each geomagnetic storm, the percentage flux change of the CR counts had its minimum value within the next 6–12 hr, which was followed by the recovery phase. During the third minor to major (G1 to G3) storm with the preceding event: 2022-08-17 02:14:00 (IP), 2022-08-17 02:14:00 (CME) there were two days of geomagnetic disturbances caused by the multiple CMEs passing the Earth starting on 14 August 2022. The continuous decrease of flux seen from August 17 to 19 could be due to this effect.

Along with the flux behavior of muon detectors at GSU and CHARA, and of NM in Oulu, Figure 8 also illustrates the variations of the solar wind and geomagnetic activity parameters during the time period of July 20 to 22 August 2022. One notices that all the solar wind and geomagnetic activity parameters (total magnetic fields,

Table 1
Summary of the Transient Rates of Muon and Neutron Flux Percentage Change at the Times of Three Geomagnetic Storms (Hereafter the Slopes)

	Slope in ±12 hr (%/hr)			Slope in ±6 hr (%/hr)			Slope in ±3 hr (%/hr)		
	GS1[a]	GS2[b]	GS3[c]	GS1	GS2	GS3	GS1	GS2	GS3
Muon000	−0.14	0.01	0.07	−0.38	−0.05	0.18	−0.28	0.69	−0.58
Muon002	−0.12	−0.01	−0.003	−0.20	−0.19	0.09	−0.22	−0.24	−0.32
Oulu	−0.23	−0.07	−0.08	−0.25	−0.12	−0.07	−0.38	−0.13	−0.09

Note. The rates are calculated in three time windows: ±12, ±6, and ±3 hr with respect to the geomagnetic storm times. [a]Geomagnetic Storm 1 (2022-07-23 03:59:00, G1). Preceding events: 2022-07-23 02:28:00 (IP), 2022-07-21 01:36:00 (CME). [b]Geomagnetic Storm 2 (2022-08-07 21:00:00, G1). Preceding events: 2022-08-07 00:45:00 (IP, HSS). [c]Geomagnetic Storm 3 (2022-08-17 18:00:00, G1-3). Preceding events: 2022-08-17 02:14:00 (IP), 2022-08-17 02:14:00 (CME).

densities, flow speeds, plasma temperatures) are enhanced during the geomagnetic storms and the interplanetary shock times. B_z component of the IMF is negative during the geomagnetic event development, demonstrating that the magnetic field in the arriving ICME was favorable for the development of the geomagnetic storms. The Kp index was strongly elevated during the events as well, reaching $Kp = 6$ at its peak for all three considered events. Given that all these three events were associated with interplanetary shocks detected at the L1 point (on 2022-07-23T02:28, 2022-08-07T00:45, and 2022-08-17T02:14, correspondingly, indicated in the footnotes of Table 1), a possible interpretation of the observed decreases in fluxes of muon and neutron detectors is their relation to the Forbush decrease effect (Janvier et al., 2021), a result of an interplanetary CME passing by the Earth and deflecting an additional fraction of cosmic rays by an embedded magnetic field. Overall we can conclude that the fluxes measured by muon detectors (both Muon000 and Muon002) are sensitive to space weather-related events.

We have also analyzed the correlations between the CR fluxes and solar wind parameters. For this short-term analysis, Pearson correlation coefficients between the flux variations of all detectors and the considered solar parameters were calculated. The CR fluxes were found to be weakly (but statistically significant) anti-correlated with flow speed and plasma temperature, whereas the weak positive correlation coefficients were observed for correlations with Dst and density. Among the two muon detectors, Muon002 was found to be more sensitive to solar wind parameters and had correlation coefficients of −0.42 and −0.27 between the muon flux change and the flow speed and temperature, respectively. These values are close to the Oulu NM values which were −0.54 and −0.3, respectively.

4. Summary and Outlook

In this paper, an exploratory study is carried out to assess the feasibility and sensitivity of a global CR muon detector network for monitoring space weather activity. The developed muon detectors are low-cost portable solutions that can be easily deployed in any geographic location. The results are based on the data recorded by a pair of identical detectors 3,500 km apart from 24 June 2022, to the end of August 2022. The detector Muon002 is

Table 2
Summary of the Transient Rates of Muon and Neutron Flux Percentage Change at the Times of Three Interplanetary Shocks Which Caused Three Geomagnetic Storms

	Slope in ±12 hr (%/hr)			Slope in ±6 hr (%/hr)			Slope in ±3 hr (%/hr)		
	IP1[a]	IP2[b]	IP3[c]	IP1	IP2	IP3	IP1	IP2	IP3
Muon000	−0.13	−0.09	−0.05	−0.45	0.0	0.02	−0.46	0.5	−1.0
Muon002	−0.07	0.0	−0.03	−0.26	−0.19	−0.2	−0.55	−0.07	−0.24
Oulu	−0.20	−0.01	−0.03	−0.28	0.04	−0.09	−0.32	−0.04	−0.08

[a]Preceding events: 2022-07-23 02:28:00 (IP), 2022-07-21 01:36:00 (CME). [b]Preceding events: 2022-08-07 00:45:00 (IP, HSS). [c]Preceding events: 2022-08-17 02:14:00 (IP), 2022-08-17 02:14:00 (CME).

installed on Mount Wilson at an elevation of 1,740 m, and the detector Muon000 is installed at the GSU campus in Atlanta at an elevation of 320 m. The detected muon fluxes are compared to the NM measurements at the Oulu station and solar wind parameters, and their responses to three geomagnetic storms and preceding ICME events are examined. Our key observations are as follows:

1. Both muon monitor detectors installed at different locations/heights and corresponding to different geomagnetic cut-off rigidities (Rc ∼4.88 GV and Rc ∼3.65 GV for detectors on Mount Wilson, CA and Atlanta, GA, respectively) demonstrate similar patterns of their reaction to space weather events (decrease of fluxes during the geomagnetic storms, see Table 1). The muon flux decreases of the Muon000 detector are less prominent with respect to the Muon002 detector.

2. Muon fluxes measured by the Muon002 detector are strongly correlated with the NM fluxes measured at Oulu station, at much lower geomagnetic cutoff rigidity (Rc ∼ 0.8 GV). The Pearson correlation coefficient is $r = 0.68$ for these measurements. The NM fluxes and Muon000 measurements, as well as measurements of the Muon000 and Muon002 detectors, are weakly (but statistically significant) positively correlated with $r = 0.20$ and $r = 0.25$, correspondingly.

3. For the first geomagnetic storm GS1 (2022-07-23 03:59:00), the muon fluxes seem to demonstrate a decreasing trend several hours before the geomagnetic storm and ICME arrival, and the decreasing trend continues during the storm period. While no solid conclusions can be made based on one event, a possible interpretation for this reduction is the effects of the interaction of cosmic rays with the fast ICME (initiated by fast, $v = 1,355$ km/s CME) and its shock front, that is, the Forbush decrease.

4. The muon fluxes measured by the Muon002 detector (installed on Mount Wilson) are found to weakly but statistically significant (extremely low p-values i.e., $p < 0.0001$) correlate with the parameters of the interplanetary solar wind measured at L1 Lagrange point and the disturbance storm time index ($r = -0.42$, $r = -0.27$, and $r = 0.18$ with the solar wind speed, temperature, and density). These values are close to those found for the NM at Oulu station $r = -0.54$, $r = -0.30$, and $r = 0.20$, respectively.

It is evident that while reacting to space weather events, the muon detectors experience much stronger fluctuations of their signal with respect to the considered Oulu NM. There are two possible reasons for that behavior. First, there is a strong coupling of the muon fluxes to the properties of the Earth's atmosphere which we find in our following works. As pointed out above, the detector on Mount Wilson (Muon002) demonstrates a much higher correlation with the Oulu NM than the detector installed in Atlanta (Muon000). Muon002 is installed at a higher altitude with respect to sea level ($h = 1,740$ m) than the detector in Atlanta and, therefore, it has less air mass above it and has less impact on the muon fluxes measured. A second possible reason is that the geomagnetic cutoff rigidities of muon detectors (Rc ∼ 4.88 GV and Rc ∼ 3.65 GV, respectively) are yet several times larger than those of the NM at Oulu (Rc ∼ 0.8 GV) and, therefore, do not result in such a high sensitivity to space weather as for Oulu. Choosing future locations at higher altitudes of lower geomagnetic cutoff rigidities may help to confirm these possible reasons for signal volatility.

The sensitivity of the muon detectors to both the space and terrestrial weather properties represents, on one hand, a challenge to an interpretation of their signals and, on the other hand, an opportunity to build novel diagnostics and prediction capabilities. The affordability of the detector (the cost is slightly more than $1,000), its portability and compact size, and low demands on maintenance (internet/WiFi and a standard power supply) make it an ideal instrument for the expansion to the full-scale network. In the future, we plan to expand the network of muon detectors and install them at different locations for monitoring both the space and terrestrial weather properties.

Data Availability Statement

The solar wind measurements onboard NASA's Deep Space Climate Observatory (DSCOVR) mission used in this study are openly accessible via the DSCOVR Space Weather Data Portal (NOAA, 2023) The data from the Oulu neutron monitor are openly accessible via the Neutron Monitor Database (University of Oulu, 2023). The pressure and temperature data from two ground weather stations at Atlanta Intl Airport (ATL) and Los Angeles Downtown (CQT) used for the pressure and temperature correction of muon monitors are openly accessible from the Iowa Environmental Mesonet (Mesonet(IEM), 2023). The space weather indexes (Kp and Dst) were obtained from the OMNIWeb database (SPDF, 2023). The raw data and pressure temperature-corrected muon detector counts from Muon000 and Muon002 detectors are publicly available at the Zenodo (Mubashir, 2023).

References

Belov, A., Baisultanova, L., Eroshenko, E., Mavromichalaki, H., Yanke, V., Pchelkin, V., et al. (2005). Magnetospheric effects in cosmic rays during the unique magnetic storm on November 2003. *Journal of Geophysical Research*, *110*(A9), A09S20. https://doi.org/10.1029/2005ja011067

Berkova, M., Belov, A., Eroshenko, E., & Yanke, V. (2011). Temperature effect of the muon component and practical questions for considering it in real time. *Bulletin of the Russian Academy of Sciences: Physics*, *75*(6), 820–824. https://doi.org/10.3103/s1062873811060086

Cane, H., & Richardson, I. (2003). Interplanetary coronal mass ejections in the near-earth solar wind during 1996–2002. *Journal of Geophysical Research*, *108*(A4), 1156. https://doi.org/10.1029/2002ja009817

Cane, H., Richardson, I., & Von Rosenvinge, T. (1996). Cosmic ray decreases: 1964–1994. *Journal of Geophysical Research*, *101*(A10), 21561–21572. https://doi.org/10.1029/96ja01964

Chaffer, A., & Tedd, B. (2016). Cosmic rays and research in schools: One school's experience. *School Science Review*, *98*(363), 67–74.

De Mendonça, R., Braga, C., Echer, E., Dal Lago, A., Munakata, K., Kuwabara, T., et al. (2016). The temperature effect in secondary cosmic rays (muons) observed at the ground: Analysis of the global muon detector network data. *The Astrophysical Journal*, *830*(2), 88. https://doi.org/10.3847/0004-637x/830/2/88

De Mendonça, R., Raulin, J.-P., Echer, E., Makhmutov, V., & Fernandez, G. (2013). Analysis of atmospheric pressure and temperature effects on cosmic ray measurements. *Journal of Geophysical Research: Space Physics*, *118*(4), 1403–1409. https://doi.org/10.1029/2012ja018026

Dmitrieva, A., Astapov, I., Kovylyaeva, A., & Pankova, D. (2013). Temperature effect correction for muon flux at the earth surface: Estimation of the accuracy of different methods. *Journal of Physics: Conference Series*, *409*, 012130. https://doi.org/10.1088/1742-6596/409/1/012130

Dorman, L. I. (2004). *Cosmic rays in the Earth's atmosphere and underground* (Vol. 303). Springer Science & Business Media.

Dvornikov, V., Sdobnov, V., & Sergeev, A. (1988). Anomalous variations of cosmic rays in the 2-5 gv rigidity range and their relation to heliospheric disturbances. *Izvestiya Akademii Nauk SSSR - Seriya Fizicheskaya*, *52*(12), 2435–2437.

Firoz, K., Kumar, D., & Cho, K.-S. (2010). On the relationship of cosmic ray intensity with solar, interplanetary, and geophysical parameters. *Astrophysics and Space Science*, *325*(2), 185–193. https://doi.org/10.1007/s10509-009-0181-9

Gleeson, L. J., & Axford, W. (1968). The solar radial gradient of galactic cosmic rays. *Canadian Journal of Physics*, *46*(10), S937–S941. https://doi.org/10.1139/p68-388

Gopalswamy, N., Xie, H., Yashiro, S., Akiyama, S., Mäkelä, P., & Usoskin, I. G. (2012). Properties of ground level enhancement events and the associated solar eruptions during solar cycle 23. *Space Science Reviews*, *171*(1–4), 23–60. https://doi.org/10.1007/s11214-012-9890-4

Guhathakurta, M. (2021). Everyday space weather. *Journal of Space Weather and Climate*, *11*, 36. https://doi.org/10.1051/swsc/2021019

He, X., Butler, C., Syed, S., Potdevin, E., Tarrant, P., Chen, N., & Wei, T. (2021). Development and production of modular cosmic ray telescopes. In *Proc. 37th ICRC*.

Jansen, F., Munakata, K., Duldig, M., & Hippler, R. (2001). Muon detectors–the real-time, ground based forecast of geomagnetic storms in Europe. In *ESA space weather workshop: Looking towards a european space weather programme*.

Janvier, M., Démoulin, P., Guo, J., Dasso, S., Regnault, F., Topsi-Moutesidou, S., et al. (2021). The two-step Forbush decrease: A tale of two substructures modulating galactic cosmic rays within coronal mass ejections. *The Astrophysical Journal*, *922*(2), 216. https://doi.org/10.3847/1538-4357/ac2b9b

Kobelev, P., Belov, A., Mavromichalaki, E., Gerontidou, M., & Yanke, V. (2011). Variations of barometric coefficients of the neutron component in the 22-23 cycles of solar activity. In *Proc. 32nd ICRC*.

Kojima, H., Antia, H., Dugad, S., Gupta, S., Jagadeesan, P., Jain, A., et al. (2015). Dependence of cosmic ray intensity on variation of solar wind velocity measured by the grapes-3 experiment for space weather studies. *Physical Review D*, *91*(12), 121303. https://doi.org/10.1103/physrevd.91.121303

Koldobskiy, S. A., Kähkönen, R., Hofer, B., Krivova, N. A., Kovaltsov, G. A., & Usoskin, I. G. (2022). Time lag between cosmic-ray and solar variability: Sunspot numbers and open solar magnetic flux. *Solar Physics*, *297*(3), 1–18. https://doi.org/10.1007/s11207-022-01970-1

Kudela, K., & Brenkus, R. (2004). Cosmic ray decreases and geomagnetic activity: List of events 1982–2002. *Journal of Atmospheric and Solar-Terrestrial Physics*, *66*(13–14), 1121–1126. https://doi.org/10.1016/j.jastp.2004.05.007

Kudela, K., Slivka, M., Stehlik, M., & Geranios, A. (1993). Cosmic-ray fluctuations and interplanetary magnetic fields. *Astrophysics and Space Science*, *199*(1), 125–132. https://doi.org/10.1007/bf00612982

Maghrabi, A., Aldosari, A., & Almutairi, M. (2021). Correlation analyses between solar activity parameters and cosmic ray muons between 2002 and 2012 at high cutoff rigidity. *Advances in Space Research*, *68*(7), 2941–2952. https://doi.org/10.1016/j.asr.2021.05.016

Mendonça, R., Wang, C., Braga, C., Echer, E., Dal Lago, A., Costa, J., et al. (2019). Analysis of cosmic rays' atmospheric effects and their relationships to cutoff rigidity and zenith angle using global muon detector network data. *Journal of Geophysical Research: Space Physics*, *124*(12), 9791–9813. https://doi.org/10.1029/2019ja026651

Mesonet(IEM), I. E. (2023). The Iowa environmental mesonet (IEM) environmental data [Dataset]. Stl. Retrieved from https://mesonet.agron.iastate.edu/

Mishra, V., & Mishra, A. (2018). Long-term modulation of cosmic-ray intensity and correlation analysis using solar and heliospheric parameters. *Solar Physics*, *293*(10), 1–22. https://doi.org/10.1007/s11207-018-1357-7

Mubashir, A. (2023). Muon000 and Muon002 raw and pressure temperature corrected data set [Dataset]. Zenodo. https://doi.org/10.5281/ZENODO.8193451

Munakata, K., Bieber, J. W., Yasue, S.-i., Kato, C., Koyama, M., Akahane, S., et al. (2000). Precursors of geomagnetic storms observed by the muon detector network. *Journal of Geophysical Research*, *105*(A12), 27457–27468. https://doi.org/10.1029/2000ja000064

Munakata, K., Kozai, M., Evenson, P., Kuwabara, T., Kato, C., Tokumaru, M., et al. (2018). Cosmic-ray short burst observed with the global muon detector network (GMDN) on 2015 June 22. *The Astrophysical Journal*, *862*(2), 170. https://doi.org/10.3847/1538-4357/aacdfe

NOAA. (2023). Deep space climate observatory (DSCOVR) space weather data portal [Dataset]. Stl. Retrieved from https://www.ngdc.noaa.gov/dscovr/portal/index.html#/

Parker, E. (1958). Cosmic-ray modulation by solar wind. *Physical Review*, *110*(6), 1445–1449. https://doi.org/10.1103/physrev.110.1445

Reames, D. V. (2021). Solar energetic particles. A modern primer on understanding sources, acceleration and propagation (Vol. *978*). https://doi.org/10.1007/978-3-030-66402-2

Sabbah, I. (2000). The role of interplanetary magnetic field and solar wind in modulating both galactic cosmic rays and geomagnetic activity. *Geophysical Research Letters*, *27*(13), 1823–1826. https://doi.org/10.1029/2000gl003760

Shrivastava, P. K., & Jaiswal, K. (2003). High-speed solar wind streams and cosmic-ray intensity variations during 1991–1996. *Solar Physics*, *214*(1), 195–200.

SPDF, N. S. P. D. F. (2023). NASA's space physics data facility (SPDF) [Dataset]. Stl. Retrieved from https://omniweb.gsfc.nasa.gov/html/ow_data.html

Storini, M. (1990). Galactic cosmic-ray modulation and solar-terrestrial relationships. *Il Nuovo Cimento - B C*, *13*(1), 103–124. https://doi.org/10.1007/bf02515780

Svensmark, H., Svensmark, J., Enghoff, M. B., & Shaviv, N. J. (2021). Atmospheric ionization and cloud radiative forcing. *Scientific Reports*, *11*(1), 19668. https://doi.org/10.1038/s41598-021-99033-1

SWPC NOAA. (2023). Space weather prediction center at national oceanic and atmospheric administration [Dataset]. SWPC NOAA. Retrieved from https://www.swpc.noaa.gov/news-archive

University of Oulu, S. G. O. (2023). Cosmic ray station sodankyla geophysical observatory neutron monitor database [Dataset]. Stl. Retrieved from https://cosmicrays.oulu.fi/

Zyla, P., Barnett, R., Beringer, J., Dahl, O., Dwyer, D., Groom, D., et al. (2020). Review of particle physics. *Progress of Theoretical and Experimental Physics*, *2020*(8), 083C01.